

**AURONES OF AMINE AND CARBAMATE
FUNCTIONALITIES AS NEUROPROTECTIVE
AGENTS WITH MULTITARGETING
POTENTIAL: SYNTHESIS,
STRUCTURE-ACTIVITY RELATIONSHIPS AND
MODE OF ACTION STUDIES**

LIEW KOK FUI

UNIVERSITI SAINS MALAYSIA

2016

**AURONES OF AMINE AND CARBAMATE
FUNCTIONALITIES AS NEUROPROTECTIVE AGENTS
WITH MULTITARGETING POTENTIAL: SYNTHESIS,
STRUCTURE-ACTIVITY RELATIONSHIPS AND
MODE OF ACTION STUDIES**

by

LIEW KOK FUI

**Thesis submitted in fulfilment of the requirements for the Degree of
Doctor of Philosophy**

June 2016

I dedicate this thesis to the memory of my father,

To my mother,

&

To my dearest wife for always being there for me through thick and thin

ACKNOWLEDGEMENT

First and foremost, I would like to express my sincere gratitude to my main supervisor, Dr. Lee Chong Yew for his excellent guidance, patience and support that helped me in all the time of my graduate studies and writing of this thesis. I would also like to thank my co-supervisors, Prof. Chan Kit Lam and Dr. Siti Rafidah Yusof, for their insightful comments and advices, which incited me to widen my research from various perspectives.

Next, I would like to acknowledge Dr. Teh Chin Hoe and Dr. Vikneswaran Murugaiyah for their constant help and advices throughout my research. Special thanks to my seniors, Dr. Low Bin Seng and Dr. Ma Hai Qiu for their sharing of knowledge and experiences especially in the early years of my graduate studies. My gratitude also goes to Dr. Siti's research group, Aziah and Mahathir for their assistance in the blood-brain barrier studies. I extend my sincere thanks to the technical officers in School of Pharmaceutical Sciences, Universiti Sains Malaysia. My sincere appreciation also goes to my fellow colleagues and friends, Chung Wan Jie, Elaine Lee, Liew Wai Lam, Forough Ebrahimi, Saifullahi Abubakar, Lee Yuan-E, Dr. Naveen Kumar H.S and Khaw Kooi Yeong for their invaluable friendship and support that made the completion of this thesis possible. My research would not have been possible without their help and support.

I would also like to acknowledge the support by the FRGS grant awarded to Dr. Lee Chong Yew and Prof. Chan Kit Lam by the Ministry of Higher Education (MOHE) of Malaysia and Universiti Sains Malaysia. My gratitude also goes to the MyPhD Scholarship from the Ministry of Education for providing financial support throughout my graduate studies.

Last but not least, I would like to express my heartfelt gratitude to my parents and family for their unconditional support, understanding and concern throughout the course of my graduate studies. I would like to give special thanks to my wife, Cheng Lee Chuen for her endless encouragement, support and love throughout the good and bad times in my graduate studies.

Thank you all.

TABLE OF CONTENTS

	Page
Acknowledgement	ii
Table of Contents	iv
List of Tables	xi
List of Figures	xiv
List of Abbreviations	xxiv
List of Appendices	xxix
Abstrak	xxx
Abstract	xxxii

CHAPTER ONE: INTRODUCTION

1.1	Neurodegenerative diseases	1
1.1.1	Prevalence and pathogenesis of AD	2
1.1.2	Current treatment modalities for AD	3
1.1.3	Emerging paradigm: Multitarget-directed ligand (MTDL)	5
1.1.4	The importance of drug-like properties	10
1.2	Overview of aurones and their AD-related activities	13
1.3	Problem statement and hypotheses	15
1.4	Objectives of study	17

CHAPTER TWO: DESIGN AND SYNTHESIS OF TARGET COMPOUNDS

2.1	Introduction	18
2.2	Rationale of target compound design	18
2.3	Chemical consideration	26
2.4	Structural assignment of the aurones	33
2.5	Assignment of <i>E/Z</i> configurations	41
2.6	Materials and methods	44

2.6.1	General details	44
2.6.2	General procedure for the synthesis of Series 1	45
2.6.2(a)	2', 4'-dihydroxy-2-bromoacetophenone (1-10)	45
2.6.2(b)	6-hydroxybenzofuran-3(2 <i>H</i>)-one (1-12)	45
2.6.2(c)	<i>O</i> -alkylation of 4-hydroxybenzaldehydes	46
2.6.2(d)	Condensation of 1-12 with functionalized benzaldehydes	47
2.6.3	General procedure for the synthesis of Series 2	48
2.6.3(a)	6-methoxybenzofuran-3(2 <i>H</i>)-one (2-12)	48
2.6.3(b)	Condensation of 2-12 with functionalized benzaldehydes	48
2.6.3(c)	(<i>Z</i>)-6-methoxy-2-pyridin-4-ylmethylene- benzofuran-3(2 <i>H</i>)-one (2-6)	49
2.6.3(d)	(<i>Z</i>)-2-(4-hydroxybenzylidene)-6-methoxy benzofuran-3(2 <i>H</i>)-one (2-9)	49
2.6.4	General procedure for the synthesis of Series 3	50
2.6.4(a)	(<i>Z</i>)-6-hydroxy-2-(4-methoxy-benzylidene)- benzofuran-3(2 <i>H</i>)-one (1-8)	50
2.6.4(b)	<i>O</i> -alkylation of 1-8	50
2.6.5	General procedure for the synthesis of Series 4	51
2.6.5(a)	(<i>Z</i>)-6-hydroxy-2-(3,4,5-trimethoxy-benzylidene)- benzofuran-3(2 <i>H</i>)-one (4-8)	51
2.6.5(b)	<i>O</i> -alkylation of 4-8	51
2.6.6	General procedure for the synthesis of Series 5	52
2.6.6(a)	Carbamylation of Series 1 derivatives (1-1 to 1-8 except 1-6)	52
2.6.7	General procedure for the synthesis of Series 6	52

2.6.7(a)	Condensation of 2-12 with 3-chloro-4-hydroxybenzaldehyde	52
2.6.7(b)	<i>O</i> -alkylation of 6-12	53
2.6.7(c)	Condensation of 2-12 with 2-chloro-4-hydroxybenzaldehyde	53
2.6.7(d)	<i>O</i> -alkylation of 6-14	54
2.6.8	X-ray crystallography of compound 6-1 and 6-8	54
2.6.9	High pressure liquid chromatography (HPLC) analysis	55
2.7	Summary	55

CHAPTER THREE: CHOLINESTERASE INHIBITORY

ACTIVITIES OF AURONES

3.1	Introduction	56
3.2	Materials and methods	57
3.2.1	<i>In vitro</i> inhibition studies on cholinesterase enzymes	57
3.2.2	Molecular docking	58
3.2.3	Determination of mode of enzyme inhibition of selected aurones	59
3.3	Results and discussion	60
3.3.1	<i>In vitro</i> inhibition studies on cholinesterase enzymes	60
3.3.2	Molecular docking of selected aurones with AChE and BuChE	71
3.3.3	Kinetic study of cholinesterase inhibition	81
3.4	Summary	87

CHAPTER FOUR: MULTI-TARGETING POTENTIAL OF AURONES

4.1	Introduction	89
-----	--------------	----

4.1.1	Monoamine oxidase (MAO) inhibition	89
4.1.2	Amyloid-beta ($A\beta$) aggregation inhibition	90
4.1.3	Approach for the evaluation of the aurones	91
4.2	Materials and methods	92
4.2.1	Determination of inhibitory effects on monoamine oxidase enzymes	92
4.2.2	Molecular docking for MAO-B	93
4.2.3	Determination of mode of MAO-B inhibition by selected aurone	94
4.2.4	Inhibition studies on self-induced $A\beta_{1-40}$ aggregation	95
4.2.5	Molecular docking for $A\beta$ peptide	96
4.3	Results and discussion	97
4.3.1	<i>In vitro</i> inhibition studies on the MAO enzymes	97
4.3.1(a)	Inhibition of MAO-A and MAO-B at a fixed concentration (50 μ M) of test compound	98
4.3.1(b)	Determination of IC_{50} values of selected aurones	103
4.3.2	Molecular docking of the most active aurone in MAO-B inhibition	106
4.3.3	Kinetic study of MAO-B inhibition	110
4.3.4	Inhibition studies on self-induced $A\beta_{1-40}$ aggregation	112
4.3.5	Docking studies on $A\beta$	116
4.4	Summary	121

CHAPTER FIVE: *IN VITRO* PHARMACOKINETIC STUDIES OF SELECTED AURONES AND HPLC METHOD DEVELOPMENT FOR THEIR QUANTIFICATION

5.1	Introduction	122
5.1.1	<i>In vitro</i> metabolic stability	123
5.1.2	<i>In vitro</i> BBB permeability models	123

5.2	Materials and methods	124
5.2.1	<i>In vitro</i> metabolic stability by rat liver microsomes	124
5.2.2	Development and validation of HPLC method for BBB permeability assays	126
5.2.2(a)	General details	126
5.2.2(b)	Chromatographic condition	126
5.2.2(c)	Preparation of stock solutions and working standards	128
5.2.2(d)	Pre-treatment of HPLC analysis samples	128
5.2.2(e)	Method validation	128
5.2.3	Evaluation of BBB permeability by PAMPA assay	130
5.2.4	<i>In vitro</i> porcine brain endothelial cell model	131
5.2.4(a)	PBEC culture (plate preparation)	131
5.2.4(b)	Cell viability assay	132
5.2.4(c)	PBEC bidirectional permeability assay	133
5.2.4(d)	Determination of intrinsic transcellular permeability (P_0) using multiple-pH permeability assay	135
5.2.5	Statistical Analysis	136
5.3	Results and discussion	136
5.3.1	<i>In vitro</i> metabolic stability in rat liver microsomes (RLM)	136
5.3.2	HPLC method development and validation for BBB permeability assay	143
5.3.2(a)	HPLC method validation of compounds for PAMPA-BBB assay	146
5.3.2(b)	HPLC method validation for <i>in vitro</i> PBEC-BBB assay	151

5.3.3	Evaluation of the passive permeability of aurones using the <i>in vitro</i> parallel artificial membrane permeability for blood-brain barrier (PAMPA-BBB) assay	154
5.3.4	<i>In vitro</i> porcine brain endothelial cell (PBEC) permeability model	157
5.3.4(a)	Determination of PBEC cell viability in the presence of aurones 2-2 , 2-3 , and 4-3	157
5.3.4(b)	Permeability evaluation of aurones 2-2 , 2-3 and 4-3 in PBEC bidirectional assay	159
5.3.4(c)	Derivation of the intrinsic transcellular permeability (P_0) of aurone 4-3 from apparent permeability (P_{app}) using multiple-pH permeability assay on the PBEC-BBB model	167
5.4	Summary	172

CHAPTER SIX: NEUROPROTECTIVE POTENTIAL OF A SELECTED AURONE IN *CAENORHABDITIS ELEGANS* (*C. ELEGANS*) MODELS

6.1	Introduction	174
6.1.1	A β -induced paralysis model	175
6.1.2	6-Hydroxydopamine (6-OHDA) induced neurodegeneration model	175
6.1.3	Evaluation of the neuroprotective potential of aurone 4-3	176
6.2	Materials and methods	177
6.2.1	Materials	177
6.2.2	Synthesis of the hydrochloride salt of aurone 4-3 (4-3 HCl)	178
6.2.3	<i>C. elegans</i> strains and maintenance	178

6.2.3(a)	Preparation of nematode growth medium (NGM) agar	179
6.2.3(b)	Preparation of food source (OP50)	179
6.2.3(c)	Preparation of M9 buffer solution	180
6.2.4	Preparation of test plates	180
6.2.5	A β -induced paralysis assay	181
6.2.6	6-OHDA-induced DAergic neurodegeneration assay	181
6.2.7	Statistical analysis	182
6.3	Results and discussion	183
6.3.1	Synthesis of hydrochloride salt of 4-3 (4-3 HCl)	183
6.3.2	Protective effects of 4-3 HCl against A β -induced paralysis in the transgenic strain GMC101	183
6.3.3	Protective effect offered by 4-3 HCl on the 6-OHDA-induced DAergic neurodegeneration of transgenic strain UA57	187
6.4	Summary	192
CHAPTER SEVEN: CONCLUSION AND SUGGESTIONS FOR FUTURE STUDY		194
REFERENCES		201
APPENDICES		223
LIST OF PUBLICATION AND CONFERENCES		255

LIST OF TABLES

		PAGE
Table 1.1	Selected drug-like properties and their <i>in vitro</i> methods of evaluation (Di and Kerns, 2003).	12
Table 2.1	Structures of compounds in Series 1.	21
Table 2.2	Structures of compounds in Series 2.	22
Table 2.3	Structures of compounds in Series 3.	23
Table 2.4	Structures of compounds in Series 4.	23
Table 2.5	Structures of compounds in Series 5.	24
Table 2.6	Structures of compounds in Series 6.	25
Table 2.7	¹ H and ¹³ C chemical shifts of 6-1 .	37
Table 2.8	¹ H- ¹ H COSY correlations of 6-1 .	38
Table 2.9	¹ H- ¹³ C HMBC correlations of 6-1 .	39
Table 2.10	¹ H and ¹³ C chemical shifts of the olefinic proton and carbon of the present aurones.	42
Table 3.1	AChE and BuChE inhibitory activities of the aurone derivatives.	65
Table 3.2	Binding interactions, interaction sites, and binding energy for selected aurones docked into active site gorge of <i>Tc</i> AChE and <i>h</i> BChE.	73
Table 3.3	Kinetic parameters for cholinesterase inhibition of 2-3 , 4-3 , and 6-3 .	81
Table 4.1	MAO-A and MAO-B inhibitory activities of standard drugs and negative control (0.5 % DMSO)	99
Table 4.2	MAO-B inhibitory activities (IC ₅₀) of selected aurones based on percentages of inhibition > 75%.	103

Table 4.3	Binding interactions, interaction sites, and binding energy for aurone 2-2 and MAOI pargyline docked into the active site gorge of <i>h</i> MAO-B.	107
Table 4.4	Kinetic parameters for 2-2 on the MAO-B inhibition.	110
Table 4.5	A β anti-aggregation activity of test compounds at 24 h.	115
Table 4.6	Binding interactions, interaction sites, and binding energy for selected compounds docked to <i>h</i> A β ₁₋₄₀ .	118
Table 5.1	HPLC analysis conditions to quantify test compounds.	127
Table 5.2	Rat liver microsomal stability of selected active aurones.	138
Table 5.3	Calibration results, LOQ and LOD values of caffeine and theophylline by HPLC-UV detection in PBS.	146
Table 5.4	Calibration results, LOQ and LOD values of donepezil and selected aurones by HPLC-fluorescence detection in PBS.	147
Table 5.5	Recovery, within-day and between-day precision and accuracy values for caffeine, theophylline, donepezil and selected aurones in PBS.	148
Table 5.6	Calibration results, LOQ and LOD values of donepezil and selected aurones by HPLC-fluorescence detection in PBS.	152
Table 5.7	Recovery, within-day and between-day precision and accuracy values for caffeine, theophylline, donepezil and selected aurones in DMEM.	153
Table 5.8	Permeability of controls in the PAMPA-BBB assay.	156
Table 5.9	PAMPA-BBB permeability of tested aurones.	157
Table 5.10	Mean <i>P</i> _{app} , efflux ratio and percentage recovery of test compounds.	161
Table 5.11	Mean <i>P</i> _{app} , efflux ratio and percentage recovery of multiple-pH assay of aurone 4-3 , sucrose (paracellular marker), propanolol (ABL marker).	170

Table 6.1	Quantitative analysis of A β -induced paralysis in GM101. The paralysis assays were quantified for mean duration at which 50% worms were paralysed (PT ₅₀) from the transgenic worms fed with or without 4-3 HCl . <i>P</i> values are for comparisons between PT ₅₀ of untreated control versus each concentration of 4-3 HCl .	185
-----------	---	-----

LIST OF FIGURES

		PAGE
Figure 1.1	Chemical structures of clinically used drugs for the treatment of AD.	5
Figure 1.2	A simplified diagram showing the multiple factors implicated in the pathogenesis of AD and the present drugs available to address them.	6
Figure 1.3	Structure of tacrine heterodimers with promising AChE and A β aggregation inhibitory activity (Tang <i>et al.</i> , 2011).	7
Figure 1.4	Structure of tacrine-donepezil hybrid compound with selective AChE and AChE-induced A β aggregation inhibitory activities (Camps <i>et al.</i> , 2010).	8
Figure 1.5	Structure of donepezil-propargylamine hybrid compound with dual ChE/MAO inhibitory activity (Bolea <i>et al.</i> , 2011).	9
Figure 1.6.	The aurone scaffold.	13
Figure 1.7	Aurones with reported acetylcholinesterase inhibitory activity.	14
Figure 1.8	Selected structural motifs (basic amine and carbamate) from donepezil and rivastigmine used in the present study.	16
Figure 2.1	The aurone scaffold and the structures of AChEIs donepezil and rivastigmine.	19
Figure 2.2	Preparation of aurones via aldol condensation.	26
Figure 2.3	Mechanism of the Hoesch acylation of resorcinol to form intermediate 1-10 and subsequent ring closure to give 1-12 .	27
Figure 2.4	Mechanism of the <i>O</i> -alkylation of 4-hydroxybenzaldehyde with suitable chlorides to form 4- <i>O</i> -functionalized benzaldehydes.	28

Figure 2.5	Mechanism of the base-catalysed aldol condensation of 1-12 with functionalized benzaldehyde to afford Series 1 aurone followed by the carbamylation reaction with diethylcarbamyl chloride under basic condition to obtain Series 5 aurone.	30
Figure 2.6	Acid-catalysed aldol condensation to prepare an aurone.	31
Figure 2.7	Structure of 6-1 .	34
Figure 2.8	^1H spectrum of 6-1 .	35
Figure 2.9	^{13}C spectrum of 6-1 .	36
Figure 2.10	^1H - ^1H COSY spectrum of 6-1 .	38
Figure 2.11	^1H - ^{13}C HMBC spectrum of 6-1 .	40
Figure 2.12	<i>Z</i> and <i>E</i> isomers of an aurone.	41
Figure 2.13	X-ray structure of 6-8 .	43
Figure 2.14	X-ray structure of 6-1 .	44
Figure 3.1	The chemical mechanism underlying the Ellman assay.	60
Figure 3.2	Comparison of the enzyme activity for the blank control (assay buffer) and negative control (1 % PEG-400) of AChE (A) and BuChE (B) expressed in percentage (%). Determinations were done in three independent assay (n = 3). Error bars = SEM.	62
Figure 3.3	Structures of donepezil and rivastigmine.	62
Figure 3.4	Representative percentage inhibition versus concentration curves for aurones 2-3 , 4-3 , and 6-3 for AChE inhibitory activity. Datapoints are means of % inhibition \pm standard errors of means (n = 3).	63
Figure 3.5	Representative percentage inhibition versus concentration curves for aurones 2-3 , 4-3 , and 6-3 for BuChE inhibitory activity. Datapoints are means of % inhibition \pm standard errors of means (n = 3).	64

Figure 3.6	The prevalence of piperidine- and pyrrolidine-bearing aurones across Series 2 to 6 having submicromolar AChE inhibition. IC ₅₀ values are in parentheses.	67
Figure 3.7	Comparison between carbamate-bearing aurones to deduce the role and position of the moiety in affecting AChE inhibitory activities of the scaffold. IC ₅₀ values are in parentheses. An IC ₅₀ > 100 μ M is considered as inactive.	70
Figure 3.8	Types of protein-ligand bond interactions featured in the molecular docking of selected aurones onto the active site of AChE.	72
Figure 3.9	Binding modes of aurones 2-3 docked to <i>Tc</i> AChE.	76
Figure 3.10	Binding modes of aurones 4-3 docked to <i>Tc</i> AChE.	77
Figure 3.11	Binding modes of aurones 6-3 docked to <i>Tc</i> AChE.	77
Figure 3.12	Binding modes of donepezil docked to <i>Tc</i> AChE.	78
Figure 3.13	Binding mode of 4-3 docked to <i>h</i> BuChE.	80
Figure 3.14	Lineweaver-Burk plot of 2-3 on AChE inhibition. Datapoints are means of 1/V \pm standard errors of means (n = 3).	82
Figure 3.15	Secondary plot of Lineweaver-Burk plot for aurone 2-3 on AChE inhibition. Datapoints are means of y-intercept \pm standard errors of means (n = 3).	82
Figure 3.16	Lineweaver-Burk plot of 4-3 on AChE inhibition. Datapoints are means of 1/V \pm standard errors of means (n = 3).	83
Figure 3.17	Secondary plot of Lineweaver-Burk plot for aurone 4-3 on AChE inhibition. Datapoints are means of y-intercept \pm standard errors of means (n = 3).	83
Figure 3.18	Lineweaver-Burk plot of 6-3 on AChE inhibition. Datapoints are means of 1/V \pm standard errors of means (n = 3).	84

Figure 3.19	Secondary plot of Lineweaver-Burk plot for aurone 6-3 on AChE inhibition. Datapoints are means of y-intercept \pm standard errors of means (n = 3).	84
Figure 3.20	Lineweaver-Burk plot of 4-3 on BuChE inhibition. Datapoints are means of 1/V \pm standard errors of means (n = 3).	85
Figure 3.21	Secondary plot of Lineweaver-Burk plot for aurone 4-3 on BuChE inhibition. Datapoints are means of y-intercept \pm standard errors of means (n = 3).	85
Figure 3.22	Summary of the structure-activity relationship pertaining to the anti-cholinesterase activity of aurones in the present study.	88
Figure 4.1	Oxidative deamination of a monoamine catalysed by MAO enzyme.	90
Figure 4.2	The principle underlying the peroxidase-linked continuous assay for MAO activity.	98
Figure 4.3	Structures of MAO inhibitors (clorgyline and pargyline) used in the <i>in vitro</i> assay.	99
Figure 4.4	MAO-A and MAO-B inhibitory activities expressed in percentage inhibition (n = 3) for Series 1-6 aurones at a fixed concentration of 50 μ M. (*) indicates compounds with more than 75 % inhibition.	100
Figure 4.5	Representative aurones with percentages of inhibition in MAO-B activity at concentration of 50 μ M.	101
Figure 4.6	Comparison of representative aurones (Series 2 versus Series 6) showing a decrease in MAO-B inhibitory activity (percentages of inhibition are in parentheses).	102
Figure 4.7	A representative percentage inhibition versus concentration curve to determine IC ₅₀ for MAO-B inhibitory activity. The curve for aurone 2-2 is shown. Datapoints are means of % Inhibition \pm standard errors of means (n = 3).	104

Figure 4.8	MAO inhibitor aurones reported in literature (Geldenhuys <i>et al.</i> , 2012; Morales-Camilo <i>et al.</i> , 2015).	105
Figure 4.9	Binding modes of aurone 2-2 docked to <i>h</i> MAO-B.	108
Figure 4.10	Binding modes of pargyline docked to <i>h</i> MAO-B.	108
Figure 4.11	Lineweaver-Burk plot of 2-2 on MAO-B inhibition. Datapoints are means of $1/V \pm$ standard errors of means ($n = 3$).	111
Figure 4.12	Secondary plot of Lineweaver-Burk plot for aurone 2-2 on MAO-B inhibition. Datapoints are means of y -intercept \pm standard errors of means ($n = 3$).	111
Figure 4.13	Structure of curcumin.	113
Figure 4.14	A β aggregation curves for test compounds over 48 h ($n = 3$).	114
Figure 4.15	Profile of A β_{1-40} (PDB: 1BA4) based on the packing density (y -axis) versus the amino acid residues along the peptide (x -axis) in predicting amyloidogenic regions. Amino acid residues that have packing density values above a predetermined cutoff (dots in black) are identified as the amyloidogenic regions.	117
Figure 4.16	Key amyloidogenic regions of A β (Qin <i>et al.</i> , 2011) and the amyloidogenic regions predicted (indicated in boxes) for A β_{1-40} (PDB: 1BA4) by FoldAmyloid.	118
Figure 4.17	Binding orientations of aurone 4-3 docked onto <i>h</i> A β_{1-40} .	120
Figure 4.18	Binding orientations of curcumin docked onto <i>h</i> A β_{1-40} .	120
Figure 5.1	Flow chart of selection of the active aurones from three AD-related enzyme activities for the subsequent <i>in vitro</i> pharmacokinetic studies.	123
Figure 5.2	LC-MS of 4-3 (m/z 440.2848) and its mono-hydroxylated (m/z 456.2846) and demethylated (m/z 426.2592) metabolites in RLM incubation at 30 minutes.	140

Figure 5.3	Possible hydroxylated metabolites (m/z $M + 16$) for CYP450 metabolic alteration on 4-3 based on the monohydroxylated metabolite observed in LC-MS.	140
Figure 5.4	Possible demethylated metabolites (m/z $M - 14$) for CYP450 metabolic alteration on 4-3 based on the demethylated metabolite observed in LC-MS.	141
Figure 5.5	LC-MS of 2-2 (m/z 366.220) and its mono-hydroxylated metabolite (m/z 382.2161) in RLM incubation at 10 minutes.	141
Figure 5.6	Possible hydroxylated metabolites (m/z $M + 16$) for CYP450 metabolic alteration on 2-2 based on the monohydroxylated metabolite observed in LC-MS.	142
Figure 5.7	HPLC-fluorescence chromatogram of a representative aurone 2-3 (Retention time (t_R) = 4.5 min) in PBS at 400 nm (ex) and 460 nm (em).	144
Figure 5.8	HPLC-fluorescence chromatogram of (A) blank DMEM with added 25 mM HEPES and 0.1 % BSA and (B) Representative aurone 2-3 (t_R = 4.5 min) in DMEM with added 25 mM HEPES and 0.1 % BSA (ex = 400 nm, em = 460 nm).	145
Figure 5.9	PAMPA apparatus for passive permeability assay.	155
Figure 5.10	Reduction of MTT to dark purple formazan product.	158
Figure 5.11	Percentage (%) cell viability of PBEC cells after treatment with 0.5 % DMSO, donepezil, 2-2 , 2-3 and 4-3 at 30 μ M. Data presented as means of % cell viability \pm standard errors of means from three independent experiments with at least three replicate for each experiment ($n = 3$).	159
Figure 5.12	PBEC-BBB apparatus set up: (A) permeability for apical to basolateral direction, (B) permeability for basolateral to apical direction.	161

Figure 5.13	Apparent permeability coefficients, P_{app} (A to B) and P_{app} (B to A) for aurone 2-2 . Permeation studies were performed in triplicate in three independent experiments. Data are expressed as mean $P_{app} \pm \text{SEM}$ ($\times 10^{-6}$ cm/s). Efflux ratio (ER) was calculated by the equation $P_{app} \text{ (B-A)}/P_{app} \text{ (A-B)}$. Statistical significance of differences was tested by Student's t-test. The P_{app} (A to B) was significantly higher than P_{app} (B to A) at $p < 0.01$ ($p = 0.0087$), indicating an active uptake mechanism.	163
Figure 5.14	Apparent permeability coefficients, P_{app} (A to B) and P_{app} (B to A) for aurone 2-3 . Permeation studies were performed in triplicate in three independent experiments. Data are expressed as mean $P_{app} \pm \text{SEM}$ ($\times 10^{-6}$ cm/s). Efflux ratio (ER) was calculated by the equation $P_{app} \text{ (B-A)}/P_{app} \text{ (A-B)}$. Statistical significance of differences was tested by Student's t-test. The P_{app} (A to B) was significantly higher than P_{app} (B to A) at $p < 0.0001$, indicating an active uptake mechanism.	163
Figure 5.15	Apparent permeability coefficients, P_{app} (A to B) and P_{app} (B to A) for aurone 4-3 . Permeation studies were performed in triplicate in three independent experiments. Data are expressed as mean $P_{app} \pm \text{SEM}$ ($\times 10^{-6}$ cm/s). Efflux ratio (ER) was calculated by the equation $P_{app} \text{ (B-A)}/P_{app} \text{ (A-B)}$. Statistical significance of differences was tested by Student's t-test. The P_{app} (A to B) significantly higher than P_{app} (B to A) at $p < 0.05$ ($p = 0.0128$), indicating an active uptake mechanism.	164
Figure 5.16	Apparent permeability coefficients, P_{app} (A to B) and P_{app} (B to A) for donepezil. Permeation studies were performed in triplicate in three independent experiments. Data are expressed as mean $P_{app} \pm \text{SEM}$ ($\times 10^{-6}$ cm/s). Efflux ratio (ER) was calculated by the equation $P_{app} \text{ (B-A)}/P_{app} \text{ (A-B)}$. Statistical significance of differences was tested by Student's t-test. No significant difference at $p < 0.05$, indicating passive permeation.	164

Figure 5.17	Apparent permeability coefficients, P_{app} (A to B) and P_{app} (B to A) for digoxin (a P-gp substrate involving efflux mechanism). Permeation studies were performed in triplicate in three independent experiments. Data are expressed as mean $P_{app} \pm SEM$ ($\times 10^{-6}$ cm/s). Efflux ratio (ER) was calculated by the equation $P_{app} (B-A)/P_{app} (A-B)$. Statistical significance of differences was tested by Student's t-test. The P_{app} (B to A) significantly higher than P_{app} (A to B) at $p < 0.05$ ($p = 0.0367$), indicating an active efflux transport.	165
Figure 5.18	Apparent permeability coefficients, P_{app} (A to B) and P_{app} (B to A) for sucrose (a paracellular marker). Permeation studies were performed in triplicate in three independent experiments. Data are expressed as mean $P_{app} \pm SEM$ ($\times 10^{-6}$ cm/s). Efflux ratio (ER) was calculated by the equation $P_{app} (B-A)/P_{app} (A-B)$. Statistical significance of differences was tested by Student's t-test. No significant difference between the P_{app} values at $p < 0.05$, indicating a passive paracellular permeation.	165
Figure 5.19	Blood-brain barrier (BBB) <i>in vivo</i> and <i>in vitro</i> . (A) Aqueous boundary layer (ABL) is minimal due to a high velocity capillary blood flow. (B) Presence of ABL adjacent to the cell membrane due to inefficient stirring during permeability assay.	168

Figure 5.20	Derivation of the intrinsic transcellular permeability, P_0 from apparent permeability, P_{app} of aurone 4-3 using pK_a^{FLUX} method in <i>pCEL-X</i> software. The P_{app} measured for aurone 4-3 were analyzed to derive the P_0 value corrected for aqueous boundary layer (ABL) effect and paracellular permeability. The black round dots are the $\log P_{app}$ is the logarithm of measured P_{app} of aurone 4-3 . Permeability through the ABL, $\log P_{ABL}$ was determined using [3H] propanolol permeability as marker. The filter limits, $\log P_{filter}$ were from porosity of blank polycarbonate filter membrane without cells. Paracellular permeability, $\log P_{para}$, was determined using [^{14}C]sucrose permeability. Transcellular permeability, $\log P_c$ was generated with the curve maximum indicating the intrinsic transcellular permeability in logarithm, $\log P_0$ of aurone 4-3 . The sigmoidal solid curves (\log permeability-pH) were fitted to the measured $\log P_{app}$ and simultaneously refined with the fixed contributors: P_{ABL} , P_{filter} and P_{para} by a weighted nonlinear regression to derive intrinsic transcellular permeability, P_0 . Each data point was determined from three independent experiments and each experiment with $n = 3$ filter inserts.	171
Figure 6.1	Structure of aurone 4-3	177
Figure 6.2	Diagram showing the drug treatment (4-3 HCl) schedule and scoring of the paralysis assay.	184
Figure 6.3	Effects of 4-3 HCl on the $A\beta$ -induced paralysis in GMC101. Time refers to hours after temperature up-shift. Incorporation of 4-3 HCl into the agar media delayed the onset of paralysis, also suppressed the $A\beta$ -induced paralysis (untreated vs. 100 μ M, $p < 0.0001^{***}$; untreated vs. 50 μ M, $p < 0.0001^{***}$; untreated vs. 25 μ M, $p = 0.0045^{**}$, paired log rank survival test). Data are expressed as percentage of non-paralysed worms from at least three independent assays of > 100 worms in each experiment ($n = 3$). The plot shown is representative of three experiments. Error bars = SEM.	185
Figure 6.4	Diagram illustration showing the drug administration (4-3 HCl) time period and scoring of the neuronal death.	188

Figure 6.5	Representative images of the head region of worms with GFP expression pattern of DAergic neurons of <i>C. elegans</i> strain UA57, (A) worms with intact DAergic neurons, and (B-C) worms with patterns of DAergic neurons lost or degenerated. The left side shows the fluorescence images. The right side shows the differential interference contrast (DIC) images.	188
Figure 6.6	Quantification of worms with intact DAergic neurons (without neurotoxin exposure). The transgenic strain UA57, raised in the presence or absence of 4-3 HCl (25, 50 and 100 μ M) on NGM plates from synchronized eggs to L1 stage for 19 h and further incubated for 72 h without the exposure to 6-OHDA. Data were presented as the mean percentage of worms with intact DAergic neurons from at least three independent assays (n = 3) of > 100 worms in each experiment. Error bars = SEM.	189
Figure 6.7	Quantification of worms with intact DAergic neurons. The L1 worms of the transgenic strain UA57, raised in the presence or absence of 4-3 HCl (25, 50 and 100 μ M) from synchronized eggs, were exposed to the 6-OHDA and further incubated for 72 h in the presence or absence of 4-3 HCl (25, 50 and 100 μ M). Data were presented as the mean percentage of worms with intact DAergic neurons from at least three independent assays of >100 worms in each experiment. Error bars = SEM. A hash (#) indicates significant differences between 6-OHDA-treated and untreated animals ($p < 0.0001$); an asterisk (*) indicates significant differences between the 6-OHDA-treated control and 4-3 HCl + 6-OHDA-treated samples (* $p < 0.05$, **** $p < 0.0001$).	190
Figure 7.1	Aurones 2-2 and 4-3 with multitargeting potential.	196
Figure 7.2	Proposed new “fluoroaurones” based on 4-3 .	200

LIST OF ABBREVIATIONS

μCi	Microcurie
^{13}C	Carbon-13
^1H	Proton
6-OHDA	6-Hydroxydopamine
Å	Angstrom
ABL	Aqueous boundary layer
AChE	Acetylcholinesterase
AChEI	Acetylcholinesterase inhibitor
AChEIs	Acetylcholinesterase inhibitors
AD	Alzheimer's disease
ADE	Anterior deirid
ADMET	Absorption, distribution, metabolism, elimination and toxicity
ADT	AutoDockTools
ANOVA	Analysis of variance
A β	Amyloid-beta
A β_{1-40}	Amyloid-beta 1-40 peptide
A β_{1-42}	Amyloid-beta 1-42 peptide
BBB	Blood-brain barrier
BSA	Bovine serum albumin
BuChE	Butyrylcholinesterase
<i>C.elegans</i>	<i>Caenorhabditis elegans</i>
CE	Capillary electrophoresis
CEP	Cephalic
ChE	Cholinesterase
CNS	Central nervous system
CNS –	Low BBB permeation
CNS +	High BBB permeation

CNS +/-	Uncertain BBB permeation
COSY	Correlation spectroscopy
CYP450	Cytochrome P450
C β	Exocyclic olefinic carbon
Da	Dalton
DAergic	Dopaminergic
DAT-1	Dopamine transporter 1
DMEM	Dulbecco's Modified Eagle's Medium
DMSO	Dimethyl sulfoxide
DRW	Dynamic range window
DTNB	5,5'-Dithiobis-(2-nitrobenzoic acid)
ER	Efflux ratios
em	Emission
ESI-MS	Electrospray Ionization Mass Spectra
ex	Excitation
FDA	Food and Drug Administration
GABA	Gamma-aminobutyric acid
GC	Gas chromatography
GFP	Green fluorescent protein
H ₂ O ₂	Hydrogen peroxide
HBSS	Hanks' balanced salt solution
HCl	Hydrogen chloride
HEPES	4-(2-hydroxyethyl)-1-piperazineethanesulfonic acid
HFIP	Hexafluoroisopropanol
hMAO-A	Human recombinant monoamine oxidase A
hMAO-B	Human recombinant monoamine oxidase B
HMBC	Heteronuclear multiple bond correlation
HPLC	High performance liquid chromatography
HRMS	High-resolution mass spectrometry

HSQC	Heteronuclear single quantum coherence spectroscopy
Hz	Hertz
IC ₅₀	Half maximal inhibitory concentration
K ₂ CO ₃	Potassium carbonate
K _i	Inhibition constant
K _m	Michaelis-Menten constant
KOH	Potassium hydroxide
L1	Larvae stage 1
LC-MS	Liquid chromatography-mass spectrometer
LOD	Limit of detection
log D _{7.4}	Distribution coefficient at pH 7.4
Log <i>P</i>	Logarithm of the octanol/water partition coefficient
LOQ	Limit of quantification
M	Molarity
M.p.	Melting point
MAO	Monoamine oxidase
MAO-A	Monoamine oxidase A
MAO-B	Monoamine oxidase B
MAOIs	Monoamine oxidase inhibitors
MeOH	Methanol
MTDL	Multitarget-directed ligand
MTDLs	Multitarget-directed ligands
Na ₂ SO ₄	Sodium sulphate
NADP	Beta-nicotinamide adenine dinucleotide phosphate
NADPH	Nicotinamide adenine dinucleotide phosphate
NFT	Neurofibrillary tangles
NGM	Nematode growth medium
NMDA	<i>N</i> -methyl- <i>D</i> -aspartate
NMR	Nuclear magnetic resonance

NQO1	NAD(P)H: quinine oxidoreductase 1
OAT	Organic cationic transporter
°C	Celcius
P_0	Intrinsic transcellular passive permeation
PAMPA	Parallel artificial membrane permeability assay
P_{app}	Apparent permeability rate
P_{ABL}	Aqueous boundary layer restriction
P_c	Transcellular restriction
P_{para}	Paracellular restriction
P_{filter}	Filter restriction
PAS	Peripheral anionic site
PBEC	Porcine brain endothelial cells
PBL	Porcine brain lipid
PBS	Phosphate buffer saline
PDB	Protein data bank
PDE	Posterior deirid
P_e	Effective permeability
PEG-400	Polyethylene glycol 400
P-gp	Permeability glycoprotein
ppm	Parts per million
PT ₅₀	Mean duration at which 50% worms were paralyzed
r^2	Correlation coefficients
RLM	Rat liver microsomes
RMSD	Root-mean-square deviation
RO5	Rule of five
RPM	Revolutions per minute
rt	Room temperature
SEM	Standard error mean
$t_{1/2}$	Half-life

TEER	Transendothelial electrical resistance
ThT	Thioflavin T
t_R	Retention time
US\$	United States dollar
UV	Ultraviolet
V_{\max}	Maximum velocity
$ZnCl_2$	Zinc chloride
α	Alpha
β	Beta
δ	Delta
μM	Micromolar
μm	Micrometre
π	Pi
Ω	Resistance

LIST OF APPENDICES

	PAGE
Appendix 1. ¹ H NMR, ¹³ C NMR, melting points, mass spectra, and HPLC purity of final compounds.	224
Appendix 2. X-ray crystal data and structure refinement for 6-1	244
Appendix 3. X-ray crystal data and structure refinement for 6-8	245
Appendix 4. Redocking analysis of the co-crystallized donepezil with AChE from <i>Torpedo californica</i> (PDB ID: 1EVE).	246
Appendix 5. Redocking analysis of the co-crystallized tabun analogue with BuChE from <i>Homo sapiens</i> (PDB ID: 2WIJ).	247
Appendix 6. Percentage MAO-A and MAO-B inhibition of aurones at fixed concentration of 50 µM.	248
Appendix 7. Redocking analysis of the co-crystallized safinamide with human MAO-B (<i>h</i> MAO-B) (PDB ID: 2V5Z).	249
Appendix 8. LC-MS conditions for the quantitation of test compounds in rat liver microsomal incubation in the <i>in vitro</i> metabolic stability assay.	250
Appendix 9. ¹ H NMR, ¹³ C NMR, melting points, mass spectra, and HPLC purity of 4-3 HCl .	253
Appendix 10. Percentage of non-paralysed <i>C.elegans</i> GMC101 worms in paralysis assay (n = 3).	254

**AURON DENGAN KEFUNGSIAN AMINA DAN KARBAMAT SEBAGAI
AGEN NEUROPROTEKTIF DENGAN POTENSI PELBAGAI SASARAN:
SINTESIS DAN KAJIAN HUBUNGAN STRUKTUR-AKTIVITI
SERTA MOD TINDAKAN**

ABSTRAK

Penyakit Alzheimer (AD) ialah penyakit kompleks pelbagai faktor melibatkan pelbagai mekanisme yang menyumbang kepada pencetusan penyakit ini. Dalam pencarian entiti kimia baru untuk menangani faktor-faktor penyebab penyakit ini, strategi rekaan ligan diarah pelbagai sasaran (MTDL) telah digunakan dalam kajian ini dengan menggabungkan motif struktur yang terpilih (pelbagai amina dan karbamat) daripada dua ubat Alzheimer yang mantap (donepezil dan rivastigmina) ke dalam perancah auron. Auron-auon ini direka berdasarkan premis bahawa perancah tersebut berpotensi digunakan untuk membangunkan suatu sebatian pelbagai sasaran yang bersaiz munasabah kecil untuk neuroprotektif sementara memelihara ciri-ciri menyerupai ubat yang baik. Dalam kajian ini, suatu siri terbitan auron yang membawa kefungsi amina dan karbamat di pelbagai kedudukan (gelang A dan/atau B) perancah telah disintesis dan dicirikan dengan menggunakan teknik-teknik spektroskopi. Auron-auon tersebut pada mulanya dinilai dalam aktiviti *in vitro* perencatan asetilkolinesterase (AChE) dan butirilkolinesterase (BuChE). Untuk mengesahkan ciri pelbagai sasaran mereka, auron tersebut dinilai dalam dua aktiviti berkaitan dengan penyakit Alzheimer (AD), iaitu perencatan monoamina oksidase

(MAO) dan pengagregatan amiloid beta ($A\beta$). Pada masa yang sama, kestabilan metabolik dan ketelapan rintangan darah-otak (BBB) auron terpilih yang poten diperiksa untuk mengenal pasti suatu sebatian optimum dengan kombinasi pelbagai potensi dan profil farmakokinetik yang baik. Kesan neuroprotektif auron **4-3** yang paling baik kemudian diperiksa dengan dua model neurodegenerasi *Caenorhabditis elegans* (*C.elegans*), iaitu kelumpuhan diaruh $A\beta$ dan neurodegenerasi diaruh 6-hidroksidopamina (6-OHDA). Kajian hubungan struktur-aktiviti mendedahkan beberapa perencat kuat AChE selektif yang membawa moiety piperidina dan pirolidina di gelang A atau B, dengan nilai-nilai IC_{50} submikromolar. Sebagai tambahan kepada aktiviti perencatan AChE mereka, potensi pelbagai sasaran telah diperhatikan dalam dua auron, iaitu auron **2-2** (perencat MAO-B) dan **4-3** (perencat pengagregatan $A\beta$). Pengeraman mikrosom hati tikus dengan auron mengenalpasti **4-3** sebagai paling stabil secara metabolik berbanding dengan auron-auron lain. Penilaian ketelapan BBB menggunakan cerakinan ketelapan membran tiruan selari (PAMPA) dan ketelapan dwiarah sel endothelium otak khinzir (PBEC) mendedahkan kesemua auron yang diuji sangat telap secara pasif merentasi BBB serta penerapan auron **4-3** adalah melibatkan mekanisme pengambilan aktif merentasi BBB. Tambahan, auron **4-3** yang menjanjikan juga menunjukkan perlindungan kepada nematod daripada ketoksikan diaruh $A\beta$ dan 6-OHDA dalam model neurodegenerasi *C.elegans*. Maka, auron **4-3** yang ditemui dalam kajian ini mewakili suatu sebatian petunjuk menyerupai ubat yang menjanjikan kepada perkembangan lanjut perancah auron sebagai agen pelbagai poten yang berpotensi untuk penyakit neurodegeneratif.

**AURONES OF AMINE AND CARBAMATE FUNCTIONALITIES AS
NEUROPROTECTIVE AGENTS WITH MULTITARGETING POTENTIAL:
SYNTHESIS, STRUCTURE-ACTIVITY RELATIONSHIPS AND
MODE OF ACTION STUDIES**

ABSTRACT

Alzheimer's disease (AD) is a complex multifactorial disease involving diverse mechanisms contributing to the onset of the disease. In the search for novel chemical entities to address the causative factors of the disease, the multitarget-directed ligand (MTDL) design strategy has been applied in the present study by incorporating selected structural motifs (various amines and carbamate) from two established Alzheimer drugs (donepezil and rivastigmine) into the aurone scaffold. These aurones were designed on the premise that the scaffold could be utilised to develop a reasonably small sized multitargeting compound (targeting cholinesterase, monoamine oxidase, and amyloid-beta aggregation) for neuroprotection while maintaining good drug-like properties. In this study, a series of aurone derivatives carrying amine and carbamate functionalities at various positions (ring A and/or B) of the scaffold was synthesized and characterized using spectroscopic techniques. These aurones were initially evaluated for their *in vitro* acetylcholinesterase (AChE) and butyrylcholinesterase (BuChE) inhibitory activities. To further substantiate their multi-targeting properties, the aurones were evaluated on two Alzheimer's disease (AD)-related activities, namely monoamine oxidase (MAO) and amyloid-beta (A β)

aggregation inhibitions. In parallel, the metabolic stability and blood-brain barrier (BBB) permeability of selected potent aurones were examined to identify an optimal compound with a combination of multipotency and favourable pharmacokinetic profile. The neuroprotective effect of the most promising aurone **4-3** was then examined on two *Caenorhabditis elegans* (*C. elegans*) neurodegeneration models, namely A β -induced paralysis and 6-hydroxydopamine (6-OHDA)-induced neurodegeneration. Structure-activity relationship study revealed several potent selective AChE inhibitors carrying piperidine and pyrrolidine moieties at ring A or B, with submicromolar IC₅₀ values. In addition to their AChE inhibitory activity, multi-targeting potential was observed in two aurones, namely aurone **2-2** (MAO-B inhibitor) and **4-3** (A β -aggregation inhibitor). Rat liver microsomal incubation of the aurones identified aurone **4-3** to be the most metabolically stable compared to the other aurones. BBB permeability evaluation using the parallel artificial membrane permeability assay (PAMPA) and porcine brain endothelial cells (PBEC) bidirectional permeability revealed all the tested aurones to be highly passive permeable across the BBB and the permeation of aurone **4-3** to involve active uptake mechanism across the BBB. In addition, the most promising aurone **4-3** also showed protection on the nematodes against both A β - and 6-OHDA-induced toxicities in the *C.elegans* neurodegeneration models. Hence, aurone **4-3** discovered in the present study represents a promising, drug-like lead for further development of the aurone scaffold as potential multi-potent agents for neurodegenerative diseases.

CHAPTER 1

INTRODUCTION

1.1 Neurodegenerative diseases

Neurodegenerative diseases are debilitating disorders characterized by progressive loss of nerve structure and function in the central nervous system (CNS). They include Alzheimer's disease (AD), Parkinson's disease, Huntington's disease, amyotrophic lateral sclerosis and multiple sclerosis. Although there are a variety of risk factors (aging, genetics, environment, and lifestyle) leading to the onset of these diseases (Nieoullon, 2011), the outcome is the same: loss of cognitive function and motor control progressing to brain atrophy and death (Brettschneider *et al.*, 2015). Despite their enormous diversity in clinical manifestations and pathogenesis, most neurodegenerative diseases share some common key features: dramatic loss of synapses and neurons and cerebral deposits of insoluble misfolded protein aggregates (Forman *et al.*, 2004). These deposits can be considered trademarks for the different neurodegenerative disorders because the main protein component involved is different in each disease (Ramanan and Saykin, 2013). In the particular case of AD, two types of protein deposits are considered to be the pathological hallmarks of the disease, namely senile plaques (also known as amyloid plaques) that are associated with extracellular amyloid beta ($A\beta$) protein (Glenner and Wong, 1984) and intracellular neurofibrillary tangles (NFT) that are composed of hyperphosphorylated tau protein (Huang and Mucke, 2012; Longo and Massa, 2004).

1.1.1 Prevalence and pathogenesis of AD

Among the various neurodegenerative diseases that have been diagnosed, AD stood out to be the most prominent in terms of prevalence and socioeconomic burden (Maslow, 2008). The disease is named after Alois Alzheimer, the pathologist who in 1907 first observed the plaques and tangles in the brains of AD patients (Forman *et al.*, 2004). It is age-related and affects approximately 5 - 8 % of people over the age of 65, 15 - 20 % of those over the age of 75, and 25 - 50 % of those over the age of 85 (Shah *et al.*, 2008). Epidemiologic studies show that around 35 million in the world are suffering from AD and this will grow to more than 100 million cases by 2050 (Aggarwal *et al.*, 2012; Thies and Bleiler, 2013). In parallel with the increase in the number of people affected with AD, the annual financial cost to society due to AD in 2010 was estimated approximately US\$ 604 billion worldwide (Wimo *et al.*, 2013) and expected to increase by the year of 2030 (Abbott, 2011), highlighting the enormous socioeconomic impact of AD.

Notwithstanding the many efforts to understand the AD pathogenesis, the precise aetiology of AD remains incomplete (Leon *et al.*, 2013). Advancements in molecular biology and immunology over the past two decades have enabled further understanding of the disease and the identification of molecular targets that mediate the pathogenesis of AD. Several theories have come into prominence to explain the aetiology of AD (Klafki *et al.*, 2006; Suh *et al.*, 2005): the cholinergic deficit hypothesis (Bartus *et al.*, 1982), the amyloid cascade hypothesis (Hardy and Allsop, 1991; Hardy and Selkoe, 2002; Karran *et al.*, 2011), oxidative stress and mitochondrial dysfunction (Garcia-Escudero *et al.*, 2013; Marcus *et al.*, 1998; Moreira *et al.*, 2010), excitotoxic and neuroinflammatory processes (Mishizen-

Eberz *et al.*, 2004) and monoaminergic abnormalities (Baker and Reynolds, 1989, Trillo *et al.*, 2013), altogether depicting a complex picture of the disease.

The cholinergic hypothesis is particularly important as it has been the cornerstone to the discovery of the present treatments for AD. This hypothesis postulates that the cognitive impairment and symptoms (dementia, memory loss) experienced by AD patients are due to the extensive loss of cholinergic neurons in certain regions of the brain such as the hypothalamus, the amygdala, and the neocortex. Drugs that can restore this cholinergic deficit in the CNS would therefore be able to slow the cognitive decline associated with the disease.

Also of prominence is the amyloid cascade hypothesis which originates from the observation of A β plaques in the AD brains. The deposition of insoluble A β fibrils amidst the neurons and the generation and aggregation of A β monomers into protofibrils and oligomers have been shown in studies *in vitro* and *in vivo* to be toxic to the neurons (Klein, 2013). The mechanisms by which A β exerts neuronal toxicity and the identification and dynamics of the different A β forms (for examples, protofibrils, soluble oligomers) that are toxic are among the most extensively studied subjects in AD research with the aim of finding a potential therapeutic targeting A β in mind (Benilova *et al.*, 2012).

1.1.2 Current treatment modalities for AD

To date, there is no efficacious treatment available that allows the recovery and reversal of the inevitable degenerative process of AD (Simoes *et al.*, 2014). Current drugs available for AD treatment in the clinic are mainly acetylcholinesterase

inhibitors (AChEIs) (Leon *et al.*, 2013) based on the cholinergic deficit hypothesis. This hypothesis arised from evidence that AD patients suffered from cognitive dysfunction because of the loss of cholinergic neurons and activity in certain parts of the brain. Thus, a drug that inhibits the hydrolysis of the cholinergic neurotransmitter acetylcholine by presynaptic acetylcholinesterase would augment cholinergic activity and relieve the symptoms of AD. Only a handful of AChEIs have been approved by the U.S. Food and Drug Administration (FDA) and launched in the market for the treatment of mild and moderate stages of AD. They are tacrine (1993), donepezil (1996), rivastigmine (2000) and galanthamine (2001) (Hong-Qi *et al.*, 2012). Tacrine was the first acetylcholinesterase inhibitor approved for the treatment of AD (Tumiatti *et al.*, 2010). However, tacrine was eventually abandoned due to its limited therapeutic use because of its poor oral bioavailability and severe adverse effects such as hepatotoxicity and gastrointestinal reactions (Alfirevic *et al.*, 2007; Mehta *et al.*, 2012).

In 2003, another drug called memantine has been approved by FDA that acts as a non-competitive antagonist of glutamate receptors (Mehta *et al.*, 2012; Rodda and Carter, 2012). This drug marks a departure from the previous AChEIs in that it has a different mechanism of action; it binds to the *N*-methyl-*D*-aspartate (NMDA) receptor to block the excitotoxic effects of elevated glutamate levels that may lead to neuronal dysfunction (Rodda and Carter, 2012).

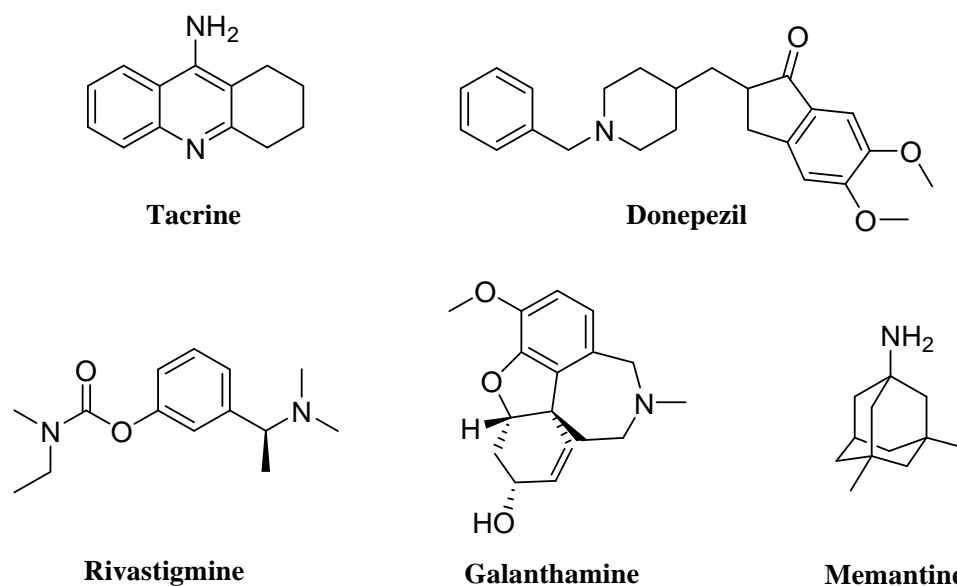


Figure 1.1: Chemical structures of clinically used drugs for the treatment of AD.

1.1.3 Emerging paradigm: Multitarget-directed ligand (MTDL)

The current drugs available for AD are considered as short-term treatments and appear to be palliative as they temporarily slow down the progressive loss of cognitive function and do not address AD's causative factors (Hong-Qi *et al.*, 2012; van Marum, 2008). The molecular basis of AD can be considered as a complex network of protein targets with multiple pathological pathways inter-relating with each other (Minarini *et al.*, 2012). Due to the multifactorial nature of AD and the diverse molecular and cellular mechanisms implicated in the disease, these “one-drug-one-target” drugs are only capable of symptomatic relief and are unable to prevent the neurodegenerative process hence the limited efficacy of the current clinical therapy for AD (Pisani *et al.*, 2011). The lack of effective treatment of the disease in spite of the complexity of AD prompted many research efforts to search for potential disease-modifying agents that target the other factors associated with AD (Citron, 2010; Galimberti and Scarpini, 2011; Salomone *et al.*, 2012). Examples of AD causative factors are amyloid-beta ($\text{A}\beta$) aggregation and generation of toxic

A β oligomers, the formation of tau protein fibrils within the neurons, neuroinflammation, excitotoxic insults, and oxidative stress (Figure 1.2). This has led to the idea of multitarget-directed ligand (MTDL) in medicinal chemistry, molecules designed to combine functionalities or moieties needed in one molecule to hit multiple targets simultaneously (Nepovimova *et al.*, 2014; Rosini *et al.*, 2005; Zhang, 2005). In principle, each of the functionalities combined in a hybrid molecule should retain their ability to interact with their corresponding targets and consequently, to produce pharmacological responses which as a whole modulate the neurodegenerative process (Cavalli *et al.*, 2008). Such an approach may hold the promise for treating a multifactorial disease such as AD.

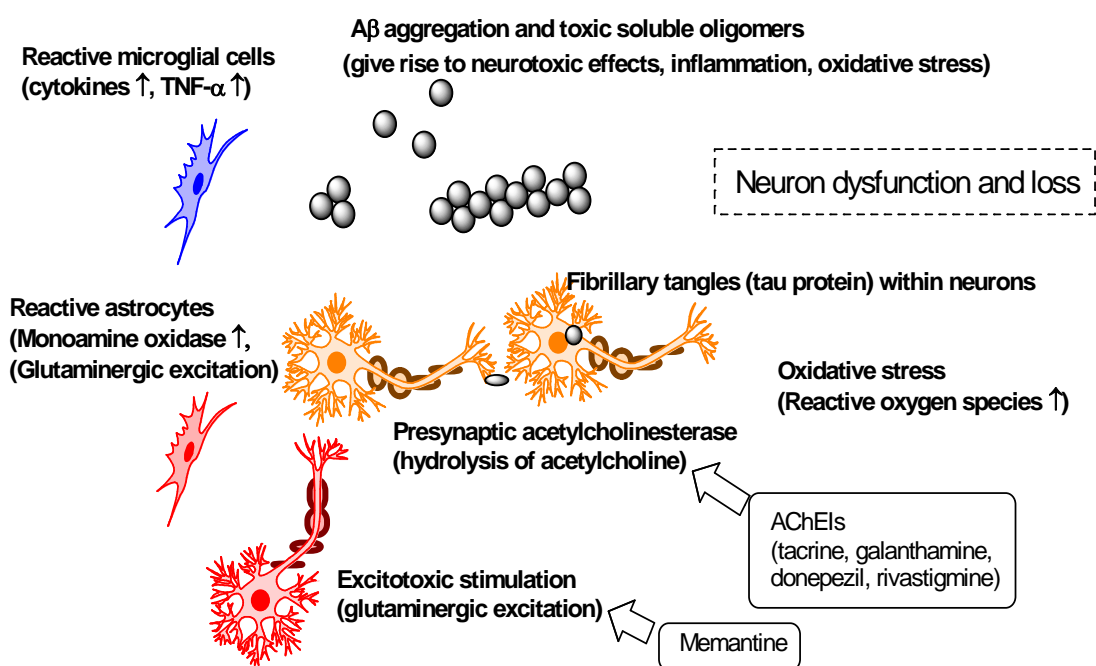


Figure 1.2: A simplified diagram showing the multiple factors implicated in the pathogenesis of AD and the present drugs available to address them.

Over the past decade, many potential multifunctional agents have been developed for AD treatment. The majority of these focused on the modifications of existing drugs with specific biological activities (Guzior *et al.*, 2015; Nepovimova *et*

al., 2014). One of the most widely adopted designs in this approach was a dual-binding AChEI in which modification was made on the existing AChEIs with additional biological properties such as A β anti-aggregating activity (Bajda *et al.*, 2011; Giacobini, 2004; Pepeu and Giovannini, 2009). Previous studies showed that the peripheral anionic site (PAS) of the enzyme acetylcholinesterase (AChE) can induce the formation of A β fibrils (Bartolini *et al.*, 2003; Inestrosa *et al.*, 1996); therefore, dual-binding AChEI that is able to bind to both the catalytic and peripheral sites of the enzyme could simultaneously inhibit the hydrolysis of acetylcholine and block the A β -aggregating action of the enzyme (Dinamarca *et al.*, 2010; Johnson and Moore, 2006). In an attempt to examine new dual-binding AChEIs, Tang and co-workers (2011) synthesized a series of novel compounds bearing tacrine and oxoisoaporphine moieties linked by an aminoalkyl tether (Figure 1.3). In this approach, tacrine acts as catalytic-site inhibitor and oxoisoaporphine as a PAS inhibitor of AChE. All the synthesized compounds were found to be AChEIs, with IC₅₀ values in the nanomolar range (3.4 to 910 nM) and showed inhibitory activities (35.5 - 85.8 %) on self-induced A β aggregation at 10 μ M (Tang *et al.*, 2011).

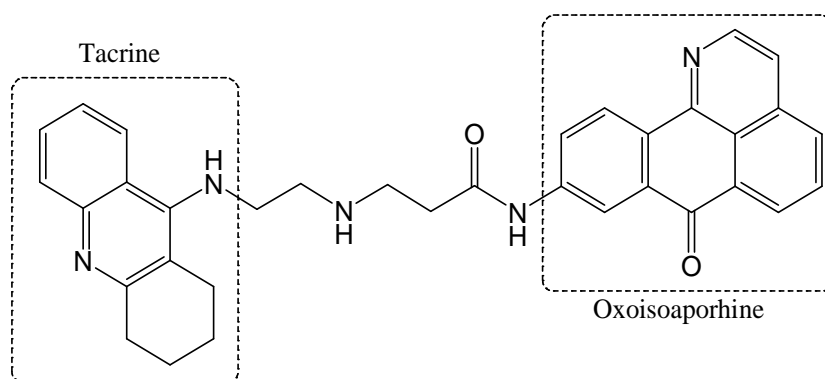


Figure 1.3: Structure of tacrine heterodimers with promising AChE and A β aggregation inhibitory activity (Tang *et al.*, 2011).

Another successful approach of multifunctional agents based on dual-binding AChEI is the donepezil-tacrine hybrid compound. In 2010, a series of AChE and A β aggregation inhibitors was synthesized by Camps and co-workers by combining both donepezil and tacrine molecules, linked by a variety of spacer subunits (Figure 1.4). All compounds of this series were able to inhibit the human AChE and butyrylcholinesterase (BuChE) in the nanomolar range together with several compounds showing multipotencies by significantly inhibiting the AChE-induced A β aggregation at the concentration of 100 μ M (Camps *et al.*, 2010).

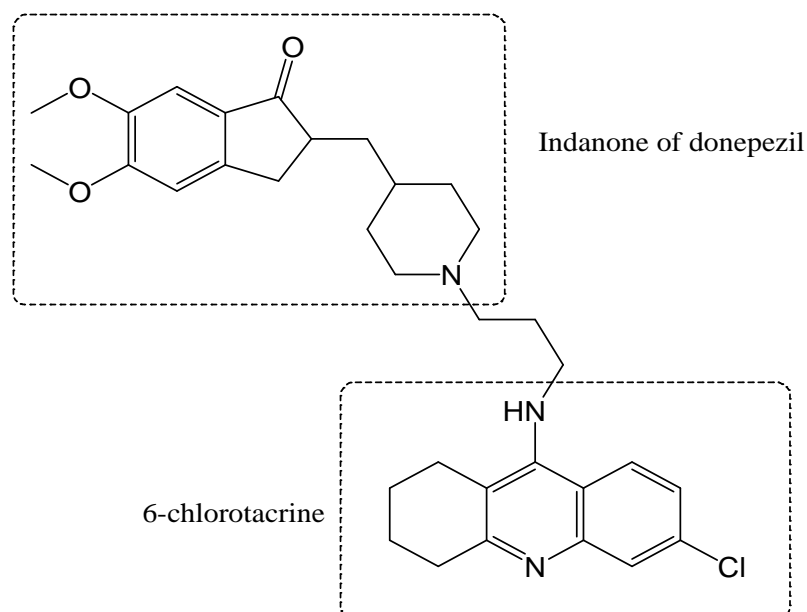


Figure 1.4: Structure of tacrine-donepezil hybrid compound with selective AChE and AChE-induced A β aggregation inhibitory activities (Camps *et al.*, 2010).

In another example, Bolea and co-workers (2011) reported a series of donepezil-based hybrid compounds capable of interacting simultaneously with cholinesterases (ChE) and monoamine oxidase (MAO), two targets related to AD and other neurodegenerative diseases. The structural design was based on the combination of the benzylpiperidine moiety of donepezil and indolylpropargyl amine

subunit present in the structure of monoamine oxidase inhibitors (MAOIs) connected by methylene chains of various lengths. Among the compounds tested, a compound (Figure 1.5) was identified as a promising compound which showed selective inhibition on monoamine oxidase A (MAO-A) with an IC_{50} of 5.2 nM and non-selective inhibition towards the cholinesterase enzymes in submicromolar range. In conjunction, this compound was also shown to be able to inhibit A β self-induced aggregation as well as AChE-induced A β aggregation. These results suggested that this compound might be a promising multitargeting drug candidate to address the multifactorial nature of AD (Bolea *et al.*, 2011).

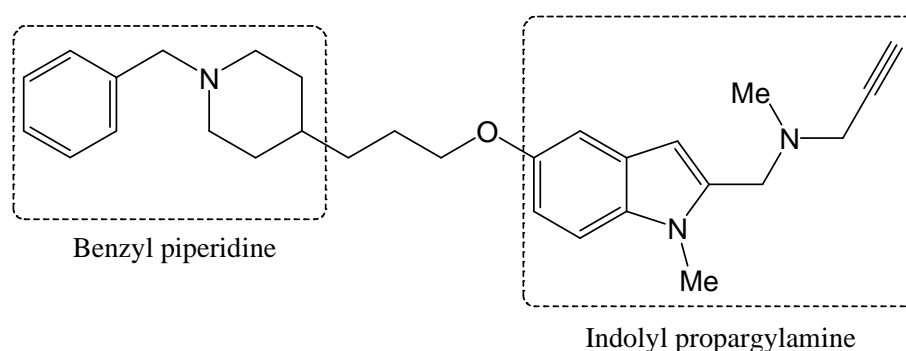


Figure 1.5: Structure of donepezil-propargylamine hybrid compound with dual ChE/MAO inhibitory activity (Bolea *et al.*, 2011).

Aside from this, more interesting multitarget-directed ligands (MTDLs) designed utilising this hybrid approach include the cholinesterase inhibitors with neuroprotective and antioxidant activity (Fernandez-Bachiller *et al.*, 2009; Samadi *et al.*, 2011), monoamine oxidase B (MAO-B) inhibitors with metal-chelating property (Fernandez-Bachiller *et al.* 2010), and metal chelators with antioxidant activity (Avramovich-Tirosh *et al.*, 2007; Zheng *et al.*, 2009). Most of these ligands have been shown to display promising biological activity *in vitro* and proved to be superior to those of one-target specific drugs. Interestingly, several studies also

suggested that MTDLs may give rise to neuroprotective effect (Bajda *et al.*, 2011; Bolea *et al.*, 2013; Minarini *et al.*, 2012). Such a desirable effect has been attributed to the combination of two or more functionalities in the hybrid molecules enabling them to intervene concertedly on several biological pathways.

1.1.4 The importance of drug-like properties

Drug discovery is a complex and demanding process, involving many disciplines and investigations into various aspects, often with complications on the road to realize a successful drug. In the earlier history of drug discovery, the trend in industry practice was to optimize the biological target activity or potency of the drug candidate first. Little attention was given to the bioavailability and pharmacokinetic properties of the potent compounds. These aspects were only addressed in the later stages of development. This was one of the reasons many compounds with high potencies failed in clinical trials due to poor pharmacokinetic profiles and bioavailability (Lipinski, 2000). In the case of drugs developed to treat CNS diseases such as AD, of the many potential compounds in development, only 2 % are able to enter the brain in sufficient concentrations to produce the desired therapeutic effect (Pardridge, 2001). These clinical failures marked a tremendous loss in terms of money, research effort, and time.

In recent years, considerable attention has been placed on assessing drug-like properties during the early phase of discovery. These drug-like properties include absorption, distribution, metabolism, elimination and toxicity (ADMET) in addition to the other physicochemical aspects to ensure the pharmacokinetic feasibility of compounds brought forth during development (Di and Kerns., 2003; Liu *et al.*,

2004). The term “drug-like” is a qualitative concept used in drug design to describe certain intrinsic properties (structural, physicochemical, biochemical and pharmacokinetic) of a compound that would contribute to its bioavailability (availability in the system) and its availability in the CNS for drugs aimed for treating CNS diseases (Kerns and Di, 2008; Li, 2005). Looking for and optimizing drug-like features in the molecules synthesized during the early part of discovery would be beneficial in ensuring quality, pharmacokinetically sound (and not any) compounds are being studied throughout the various stages of development.

Many high-throughput *in vitro* assays have been developed over the past decade for evaluating drug-like properties in order to avoid unnecessary complexities associated with animal models and to minimize the time and cost needed to screen large numbers of target compounds (Di *et al.*, 2004; Liu *et al.*, 2004). These assays measure the fundamental physicochemical and biochemical properties which determine the higher level properties such as the pharmacokinetics of a drug (Li, 2004). They include blood-brain barrier permeability assays, gastrointestinal permeability assays, plasma stability assay, solubility assay, and liver microsomal stability assay that are able to sort out candidates with acceptable drug-like properties in the earlier drug design phase with fewer resources and in a shorter amount of time (Di *et al.*, 2003; Kerns and Di, 2008; Li, 2005). Moreover, these methods also showed good correlation with *in vivo* findings and could reflect the *in vivo* pharmacokinetic condition (Li, 2005). Table 1.1 lists several commonly assessed drug-like properties and the *in vitro* assays used to evaluate them.

Table 1.1: Selected drug-like properties and their *in vitro* methods of evaluation (Di and Kerns, 2003).

Drug-like Properties	Methods/Assays
Oral/gastrointestinal permeability	Parallel Artificial Membrane Permeability Assay (PAMPA), Caco-2 cell monolayer, immobilized artificial membrane high performance liquid chromatography (HPLC), everted gut sac.
Lipophilicity	Shake flask method, reversed phase HPLC, capillary electrophoresis.
Blood-brain barrier permeability	PAMPA-BBB, cell-based method.
Metabolic stability	Liver microsomes, S9 fraction, cytosol, hepatocytes.
Toxicity	Cell toxicity, hERG block assays, zebrafish.
CYP450 inhibition and induction	Liver microsomes, hepatocytes.

In order to design a compound with drug-like properties, the Lipinski's rule of five or simply Rule of five (RO5) plays a guiding role, whereby it states that a drug-like molecule in general should have less than 5 hydrogen bond donors and 10 hydrogen bond acceptors, a molecular mass less than 500 Da, and an octanol-water partition coefficient ($\log P$) value less than 5 (Lipinski, 1997). Early evaluation of a chemical structure as suggested by the RO5 would allow one to select the possible drug candidates that would be more drug-like for further pharmacological testing (Lipinski, 2004). This rule of thumb together with the assays for evaluating drug-like properties are used to drive the design, synthesis, selection, and optimization of compounds in conjunction with the main biological activity evaluation.

1.2 Overview of aurones and their AD-related activities

Aurones (2-benzylidenebenzofuran-3-(2*H*)-ones) are small molecules belonging to the flavonoid family that are naturally present as bright yellow pigments in fruits and flowers of certain terrestrial and marine plants (Harborne *et al.*, 1988). Naturally occurring aurones derivatives are often found as their hydroxylated, methoxylated or glycosylated forms (Beney *et al.*, 2001). Although aurones are structurally related to the other subclasses of flavonoids (flavones, isoflavones and chalcones), aurones hold a unique place in nature due to the remarkably low quantities present in plants (Haudecoeur and Boumendjel, 2012).

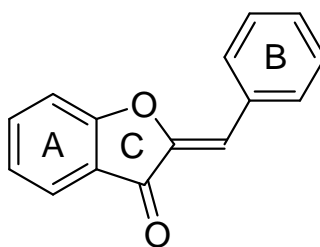


Figure 1.6: The aurone scaffold.

Ever since the first review by Boumendjel (2003), aurones have gained considerable attention as a “privileged structure” due to its promising utility in many medicinal chemistry projects (Boumendjel, 2003; Haudecour and Boumendjel, 2012; Zwergel *et al.*, 2012). Aurones have been found to possess antiproliferative effect in cancer cells (Lawrence *et al.*, 2003), anti-tyrosinase activity (Okombi *et al.*, 2006), anti-viral activity (Liu *et al.*, 2008), anti-microbial activity (Bandgar and Patil, 2010), antimalarial activity (Souard *et al.*, 2010; Carrasco *et al.*, 2014), and are potential chemopreventive agents via the induction of the cytoprotective NADP(H) Quinone Oxidoreductase 1 (NQO1) (Lee *et al.*, 2010). More recent studies revealed that aurones possess anti-inflammatory activity by reducing the production of nitric oxide

and prostaglandin E₂ (Shin *et al.*, 2011), and were potent inhibitors of the breast cancer resistance protein ABCG2 (Sim *et al.*, 2011) and Hepatitis C Virus RNA Polymerase (Haudecoeur *et al.*, 2012; Meguellati *et al.*, 2014).

Sheng and co-workers (2009) were the first to report AD related activities of synthetic aminomethylaurones through AChE inhibition. Most of the synthesized aurones demonstrated a high inhibition towards AChE with IC₅₀ in micromolar range (Sheng *et al.*, 2009). The authors also proposed that the π - π stacking interaction of an aurone planar ring system could be a reason for the enhanced AChE inhibitory activity of the aurones (Sheng *et al.*, 2009). In another investigation, a series of 6-alkoxy aurone derivatives all possessing pyridinium as the nitrogen-bearing motif showed moderate to high AChE inhibition activities (Nadri *et al.*, 2010). However, these aurones were focused mainly on the cholinesterase inhibitory activity and were not designed for multitargeting purposes. In addition, aurones have also been reported to exhibit high binding affinity for A β aggregates *in vitro* (Maya *et al.*, 2009) and more recently showing MAO inhibitory activity (Morales-Camilo *et al.*, 2015). These reported activities provide interesting leads to exploit the scaffold in the development of novel multitargeting anti-Alzheimer's agents.

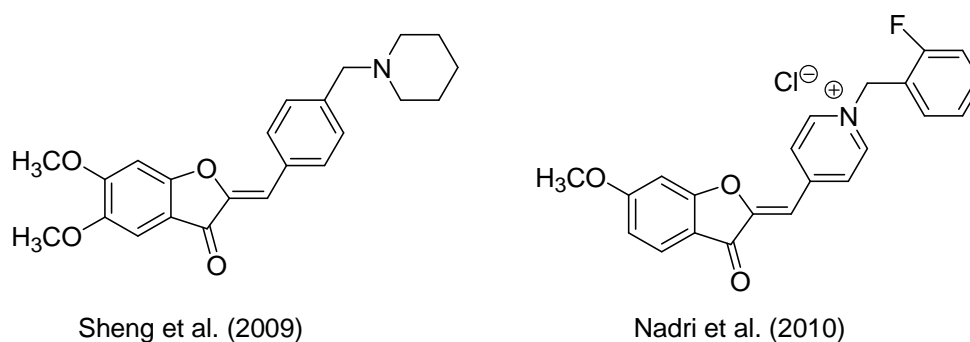


Figure 1.7: Aurones with reported acetylcholinesterase inhibitory activity.

1.3 Problem statement and hypotheses

The purpose of this thesis is to investigate the potential of aurones as neuroprotective agents via a multi-target directed ligand design while placing equal emphasis to maintain a balanced drug-like profile particularly their metabolic stability and ability to permeate the blood-brain barrier. Numerous MTDLs have been developed and were shown to have potent multi-faceted activities (Bajda *et al.*, 2011; Guzior *et al.*, 2015; Pisani *et al.*, 2011). However, despite having high potencies and strong binding affinities for their target proteins (many in the nanomolar range), these ligands were generally bulky, had high molecular weights (> 500 Da), and were tethered hybrids of two drug molecules as can be observed from several MTDL examples cited in Section 1.1.3. Such structural designs cast doubts about their drug-like properties. Large molecular weights in these compounds could hinder their ability to permeate the blood-brain barrier which is necessary for a CNS-active compound while high lipophilicity which came with their large size may attract high liver metabolism and clearance particularly by the phase 1 cytochrome P450 (CYP450) enzymes. It can be argued that in the design of these hybrid MTDLs, drug-like considerations (which are necessary for the development of CNS drugs) have been overlooked in achieving high target protein affinities and multitarget potencies.

To develop a novel multipotent anti-Alzheimer drug that retains good drug-like properties (metabolic stability and blood-brain barrier permeability), the aurone platform was utilised in the present investigation. The aurone scaffold with a tenable molecular weight of 222.24 Da and a topological polar surface area (26.3 Å²) would provide a suitable foundation for which to introduce additional key functionalities

while maintaining reasonable molecular weight and polar surface area in compliance with the RO5 (Lipinski, 1997; 2000). Over the past decade, the aurone scaffold has gained importance as a “privileged structure” due to its prevalence in many pharmacologically active compounds (Boumendjel, 2003; Zwergel *et al.*, 2012). It is proposed that by incorporating selected structural motifs (various amines and carbamate) from two established Alzheimer drugs (rivastigmine and donepezil) into the scaffold, a novel multitargeting AChEI that has additional mechanism(s) of action may be uncovered. It would also seem likely that the proposed multitargeting aurones may exhibit neuroprotective effect, as has been observed in studies on other MTDLs (Bajda *et al.*, 2011; Bolea *et al.*, 2013; Minarini *et al.*, 2012). A promising aurone obtained from this study would provide the tool to investigate this premise.

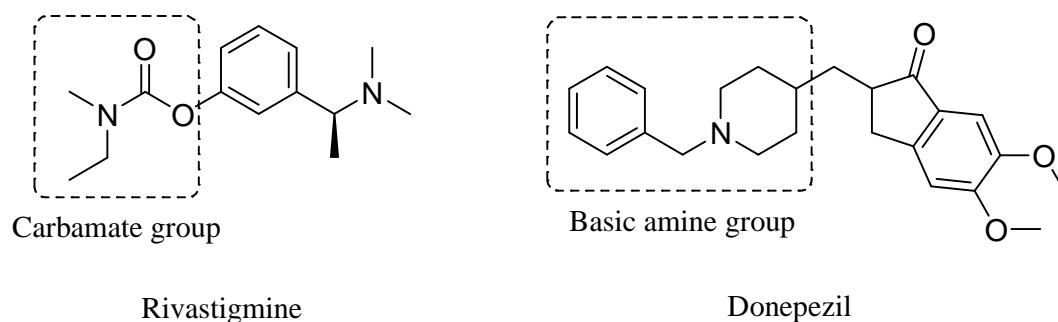


Figure 1.8: Selected structural motifs (basic amine and carbamate) from donepezil and rivastigmine used in the present study.

In addition to examining the pharmacological potential of the aurones, it is also important to gain accurate data on their drug-like properties as such information is needed to identify an optimal compound with a combination of good activity/potency and favourable pharmacokinetic profile (metabolic stability, blood-brain barrier permeability). Little is known about the drug-like properties of aurones, particularly their stability in the face of phase 1 CYP450 liver clearance and their

ability to permeate the blood-brain barrier, important features in developing a CNS-active compound. It is hypothesized that the close resemblance between the aurone's benzofuranone and the pharmacokinetically optimized donepezil's indanone might give rise to favourable drug-like properties in the target aurones in addition to their "streamlined" (small molecular weights and polar surface area) design. Furthermore, the proposed introduction of amines and carbamate moieties into the scaffold may influence the physicochemical properties of the scaffold and hence their drug-like potential.

1.4 Objectives of study

To verify the aforementioned hypotheses, the specific objectives of the study are as follow:

- (i) To design and synthesize a series of aurone derivatives incorporating the selected structural motifs from the known AChEIs donepezil and rivastigmine.
- (ii) To elucidate the structure-activity relationship of the aurones with respect to their cholinesterase inhibitory activity as well as their mode of binding.
- (iii) To investigate the multitargeting potential of the aurones in two AD-related targets (monoamine oxidase and A β aggregation) and their respective binding mechanisms.
- (iv) To evaluate the drug-like properties of selected aurones using *in vitro* pharmacokinetic assays (metabolic stability, blood-brain barrier permeability).
- (v) To investigate the neuroprotective effects of the most promising aurone in two *Caenorhabditis elegans* (*C.elegans*) neurodegeneration models.

CHAPTER 2

DESIGN AND SYNTHESIS OF TARGET COMPOUNDS

2.1 Introduction

This chapter describes the design and synthesis of target compounds for the evaluation of potential neuroprotective properties based on their anti-cholinesterase activity. These compounds possess the aurone scaffold with modifications at rings A and B with various basic amines and carbamate functionalities. The rationale underlying the design, chemical considerations of their synthesis and the experimental methods are presented. The structures of the synthesized compounds were identified by proton-1 (^1H) and carbon-13 (^{13}C) nuclear magnetic resonance (NMR) spectroscopy, and their mass spectra. Spectroscopic data, melting points, yields and purities of each compound are listed in Appendix 1.

2.2 Rationale of target compound design

The aurone scaffold was chosen in this investigation owing to the close resemblance of its benzofuranone core with the indanone of the clinically used Alzheimer drug donepezil (Figure 2.1). Donepezil is a well-tolerated, orally bioavailable acetylcholinesterase inhibitor for the treatment of AD (Sugimoto *et al.*, 2002; Wilkinson, 1999). It serves as a lead for further modifications on the aurone scaffold to uncover novel compounds with a similar pharmacokinetic profile. Furthermore, studies on a series of pyridinium aurone derivatives synthesized as acetylcholinesterase inhibitors revealed that some of these compounds exhibited high anti-cholinesterase activity (Nadri *et al.*, 2013; Nadri *et al.*, 2010). In addition,

aurones have been developed as probes for imaging A β plaques using single photon emission computed tomography (SPECT) that showed high affinity for A β aggregates (Ono *et al.*, 2007) suggesting a potential multi-targeting property in the scaffold.

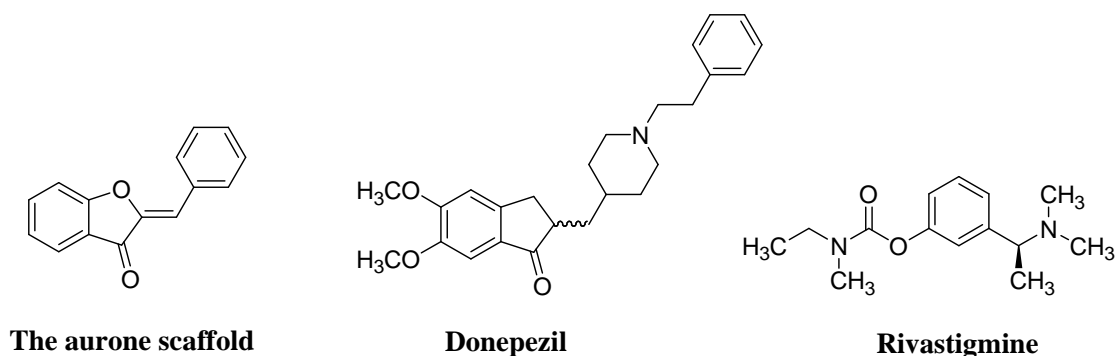


Figure 2.1: The aurone scaffold and the structures of AChEIs donepezil and rivastigmine.

In this study, a total of forty-one target compounds were synthesized and grouped into six series based on the modifications at rings A and B of the aurone scaffold. Series 1 and 2 consist of 6-hydroxyaurones and 6-methoxyaurones respectively with different substituents at the 4'-position of the ring B (Table 2.1 and 2.2). They were introduced because such oxygenated aurones have been reported to exhibit multiple bioactivities including anti-inflammatory properties (Shin *et al.*, 2011), a desirable feature in developing a multi-targeting agent. Moreover, hydroxyl and methoxyl groups would provide a good comparison between the two series with regard to their lipophilicities and hydrogen bond donor and acceptor properties. Series 3 comprises of aurones with “reversed” functionalized equivalents of Series 2 in which the various substituents are placed at the 6-position of ring A while the methoxyl group is at the 4'-position of ring B (Table 2.3). They provide suitable comparisons with Series 2 and Series 5 by which to explore the placement of the

amine or carbamate moieties at the other end of the scaffold. Series 4 aurones are akin to Series 3 with the functionalization at ring A but with a 3', 4', 5'-trimethoxy motif at ring B (Table 2.4). This modification was inspired by a report on a series of multipotent AChEIs in which the use of this motif gave rise to potent inhibitors (Belluti *et al.*, 2005). Series 5 are 6-diethylcarbamoylaurones with the amine functionalities at ring B to examine the effect of having the carbamate moiety at ring A (Table 2.5). Series 6 aurones are chlorinated equivalents of Series 2 where one chlorine is placed at positions *ortho* and *meta* to the amine functionality at ring B (Table 2.6). This series serves to assess whether the placement of an electron-withdrawing group (such as chlorine) near a potentially labile site can increase the metabolic stability of the compounds.

As for the type of substituents, they were limited to tertiary amines such as dimethylamino-, diethylamino-, pyrrolidine, and piperidine. The rationale underlying this choice was because most centrally active AChEIs such as donepezil, galanthamine and recently synthesized derivatives (Pan *et al.*, 2014; Yan *et al.*, 2012) hold basic, ionisable nitrogen-containing moieties which contribute to their activities and pharmacokinetic properties. Carbamate functionality (diethylcarbamate) borrowed from the known AChEI rivastigmine (Figure 2.1) and xanthostigmine derivatives (Rampa *et al.*, 2001) is another group introduced into the design of the present aurones. The incorporation of the aforementioned amines and carbamate to the aurone scaffold is expected to influence the anti-cholinesterase activity of the target compounds.

Table 2.1: Structures of compounds in Series 1

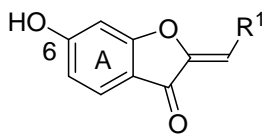
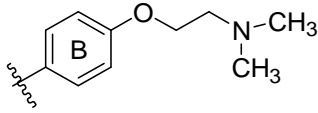
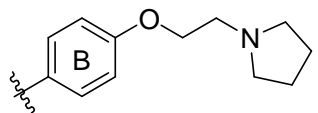
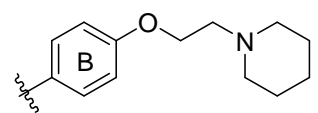
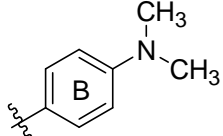
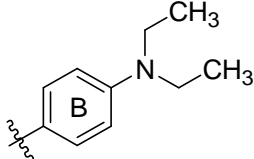
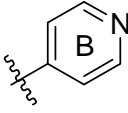
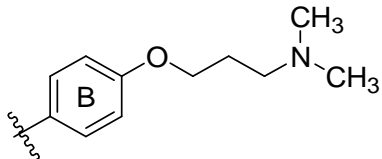
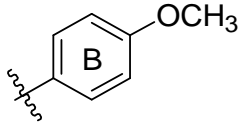
Compound	R ¹	% Yield
<i>Series 1</i> 		
1-1		63
1-2		64
1-3		59
1-4		99
1-5		81
1-6		53
1-7		84
1-8		68

Table 2.2: Structures of compounds in Series 2

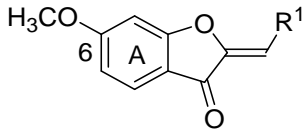
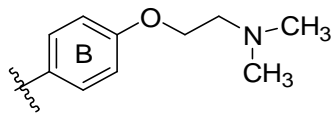
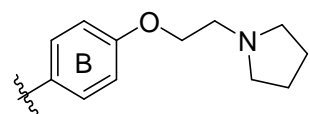
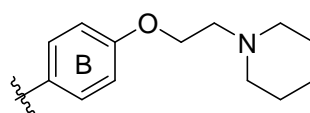
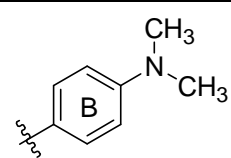
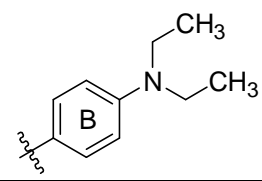
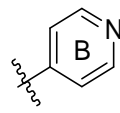
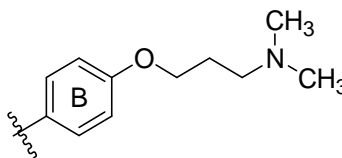
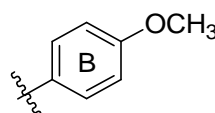
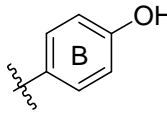
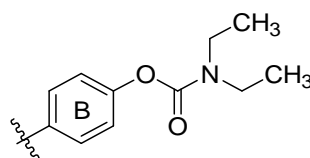
Compound	R ¹	% Yield
<p><i>Series 2</i></p> 		
2-1		53
2-2		26
2-3		19
2-4		42
2-5		47
2-6		38
2-7		33
2-8		36
2-9		98
2-11		20

Table 2.3: Structures of compounds in Series 3

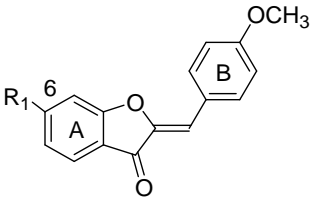
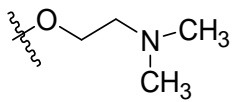
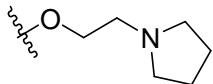
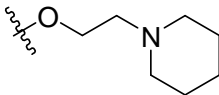
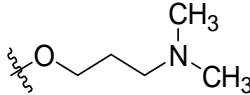
Compound	R ¹	% Yield
<i>Series 3</i> 		
3-1		46
3-2		40
3-3		46
3-7		35

Table 2.4: Structures of compounds in Series 4

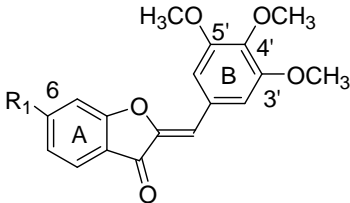
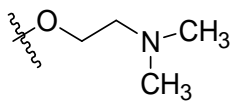
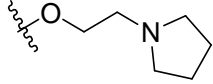
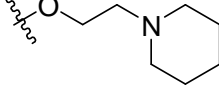
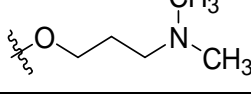
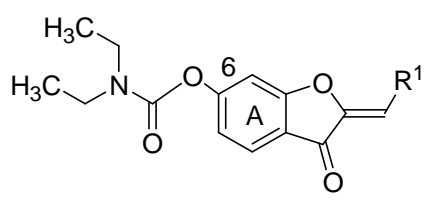
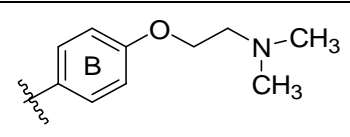
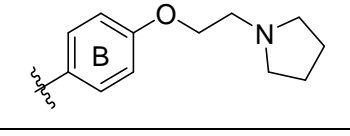
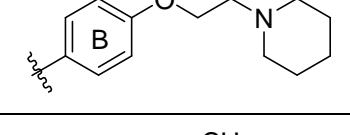
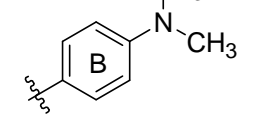
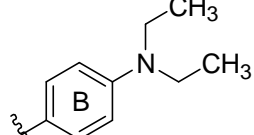
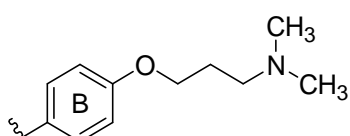
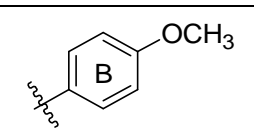
Compound	R ¹	% Yield
<i>Series 4</i> 		
4-1		42
4-2		59
4-3		70
4-7		39

Table 2.5: Structures of compounds in Series 5

Compound	R ¹	% Yield
<p><i>Series 5</i></p> 		
5-1		58
5-2		68
5-3		47
5-4		76
5-5		75
5-7		55
5-8		63